38th International Electric Vehicle Symposium and Exhibition (EVS38) Göteborg, Sweden, June 15-18, 2025

Prediction of Electrolyte Infiltration Process for Lithium-ion Battery Assisted by 3D Reconstructed Electrodes

Jixiang Cai[1,2], Jiangong Zhu[1,2,*], Mengshu Tian[1,2], Gang Wei[1,2], Wentao Xu[1,2], Haifeng Dai[1,2], Xuezhe Wei[1,2,*]

[1]*School of Automotive Studies, Tongji University, Shanghai 201804, China*

[2]*Clean Energy Automotive Engineering Center, Tongji University, Shanghai 201804, China*

[*] *Corresponding author: zhujiangong@tongji.edu.cn, weixzh@tongji.edu.cn*

Executive Summary

Electrolyte infiltration within the electrodes is of great importance to lithium-ion battery (LIB) performance. Insufficient standing time results in incomplete wetting, leading to reduced capacity and lithium plating. Meanwhile, excessive standing time causes more costs and time. To address this contradiction, this paper develops a cross-scale model to rapidly predict the electrolyte infiltration process, which extracts key structural characteristics from the 3D electrode microstructures obtained by focused ion beam-scanning electron microscope (FIB-SEM). The porosity, absolute permeability, and average pore diameter are calculated at mesoscale and imported to the macroscale model. Results show the differences between cathode and anode in the aspects of total electrolyte mass and infiltration speed. Meanwhile, it requires at least 3000 s (50 min) to achieve the complete wetting state for the researched battery. The methods described in this paper has the potential to determine the optimal standing time and accelerate the infiltration process, thus reducing the production costs and time.

1 Introduction

Lithium-ion batteries (LIBs) are the most important components in electric vehicles (EVs), energy storage systems (ESSs), and portable electronics. The huge requirements of LIBs depend on the high efficiency of battery manufacturing, which considers both product quality and cost. During the whole manufacturing process, after slurry, drying, calendaring, and assembling operations, the dry battery is obtained without electrolyte [1]. Then, the suitable electrolyte is filled and infiltrated into the pore phase. Among them, the electrolyte infiltration process is essential to battery performance and highly time-consuming [2]. Incomplete infiltration leads to lack of battery capacity and failure issues such as lithium plating [3]. On the contrary, excessive standing time significantly increases the production costs and slows down the delivery speed. Therefore, accurately estimating the suitable standing time is necessary in practical scenarios. In laboratory, the neutron imaging [4, 5], X-ray computed tomography[6], and ultrasonic scanning [7] are typically employed to visualize the infiltration process. However, these advanced instruments are challenging to use in engineering applications. Compared with experiment methods, numerical models have the advantages of cost-effective and use-convenient [8], which is able to simulate and optimize the electrolyte infiltration process.

By reviewing the existing literatures, researchers have proposed inspiring models in mesoscale and

macroscale [9]. In the aspect of mesoscale modeling, Chen et al. investigated the flow behavior within realistic pore architectures using commercial Geodict software[10], Refs. [11-13] described the utilization of lattice Boltzmann method in simulating the electrolyte wetting based on refined electrode microstructures. While these models possess advantages of high-fidelity and solid theoretical foundation, they are cost-expensive and unable to capture the characteristics of the entire electrode. In the region of macroscale modeling, Gunter et al. [14] introduced a simple model based on the momentum balance of the rise of liquid in a closed tortuous capillary which was completely an analytical solution. It fails to consider the microstructure properties which are crucial to the electrolyte infiltration behavior. In fact, models coupling mesoscale characteristics and macroscale computational efficiency are desirable. Recently, to bridge the gap between mesoscale and macroscale modeling, Chen et al. [15] and Wu et al. [16] established cross-scale models for rapid electrolyte wetting simulation. Nonetheless, they ignored the accurate calculation of absolute permeability, a key model parameter.

Thus, to address the aforementioned issues, we developed a rapid electrolyte infiltration model assisted by 3D reconstructed electrodes to realize a combination of both fidelity and computational efficiency. Firstly, assisted by the focused ion beam – scanning electron microscope (FIB-SEM), the 3D microstructures of cathode and anode were reconstructed where the active material (AM) and pore were clearly distinguished. The accuracy of these structures was validated based on porosity by conducting mercury intrusion porosimetry (MIP) tests. Then, selecting the D50 diameter, porosity, and macmullin number as key structural indicators, the representative volume elements (RVEs) of cathode and anode were determined. Based on which, the structure-related parameters required in the macroscale model, i.e., the absolute permeability and average pore diameter, were calculated at mesoscale through finite element method (FEM) and pore network model (PNM). Finally, the whole electrodes were simplified as uniformly distributed porous media, the multiphase transfer in porous media and darcy's law were defined to establish the electrolyte infiltration model. Results indicated the totally absorbed electrolyte within anode was more than cathode due to the more pore volume, the infiltration rate of anode was faster than cathode owing to the higher absolute permeability, bigger average pore diameter, and smaller contact angle. Overall, it required at least 3000 s (50 min) to get all electrodes wetted for the cathode and anode. This work offers a powerful tool to estimate the best standing time and optimize the infiltration process of LIBs and any other types of batteries.

2 Acquisition of electrode microstructure

2.1 Sample preparation and 3D reconstruction

Given that the electrolyte infiltration prediction model is a general methodology that is effective in different battery types, here, a 1.2 Ah commercial pouch lithium-ion battery with NCM523 cathode and Graphite anode was selected as a research example. After disassembling and cutting operations in the glove-box condition, the cathode and anode sheets with small size were extracted from the battery. Fig. 1 shows the microstructure reconstruction workflow of both cathode and anode. Firstly, the FIB-SEM (Fig. 1a) was utilized to obtain 2D images (Fig. 2b and 2e) step by step cross the thickness direction [17]. Then, through interactive thresholding segmentation based on greyscale value difference [18], the AM phase within electrodes (Fig. 1c and 1f) was clearly distinguished. Finally, the real microstructures of cathode (Fig. 1d) and anode (Fig. 1g) were reconstructed in 3D form. Where, the AM and pore phases are illustrated in different color. The revolution in three directions of both electrodes was all 30 nm. The volume sizes of reconstructed cathode and anode microstructures were both 40 μm × 40 μm × 40 μm.

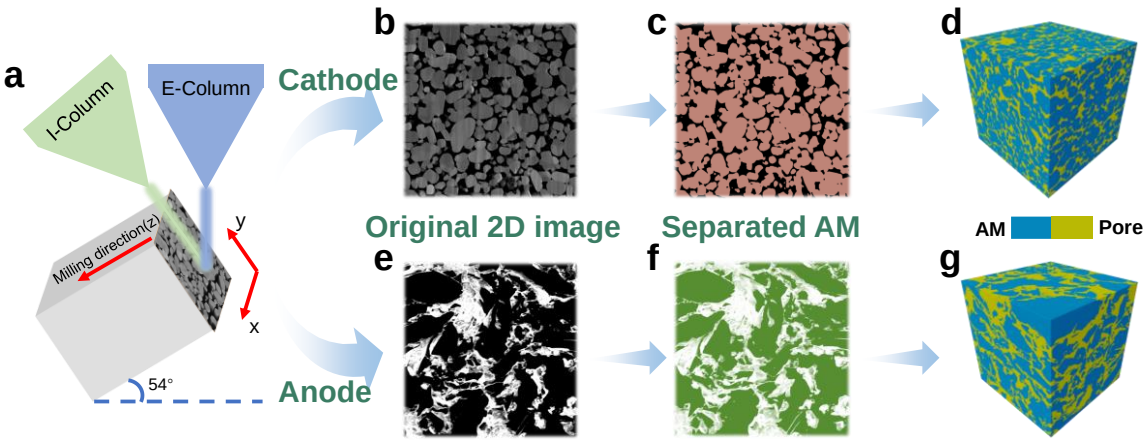

Fig. 1. Microstructure reconstruction workflow of NCM523 cathode and Graphite anode. a Schematic diagram of FIB-SEM; b-d original 2D image (b), separated AM (c), and 3D reconstruction result (d) of cathode; e-g results of anode with the same methods.

2.2 Porosity-based validation

Notably, in the process of electrodes 3D reconstruction, some subjective errors were inevitably introduced and the reconstruction accuracy ought to be further validated. Regarding this issue, comparative studies were carried out. Specifically, the porosity of cathode and anode was obtained through reconstructed microstructure (image) and MIP test (experiment), respectively. As shown in Fig. 2, the areal porosity of cathode (Fig. 2a) and anode (Fig. 2b) from separator to current collector was obtained through the analysis of the reconstructed microstructures. Based on which, the volume fractions were calculated to be 28.8% for cathode and 36.2% for anode. Simultaneously, Fig. 2 presents the experimental results of electrode volume fraction as 30.2% for cathode and 36.4% for anode. The reconstruction errors of 1.4% and 0.2% demonstrate the accuracy of the reconstructed volumes which are reliable to extract electrode parameters.

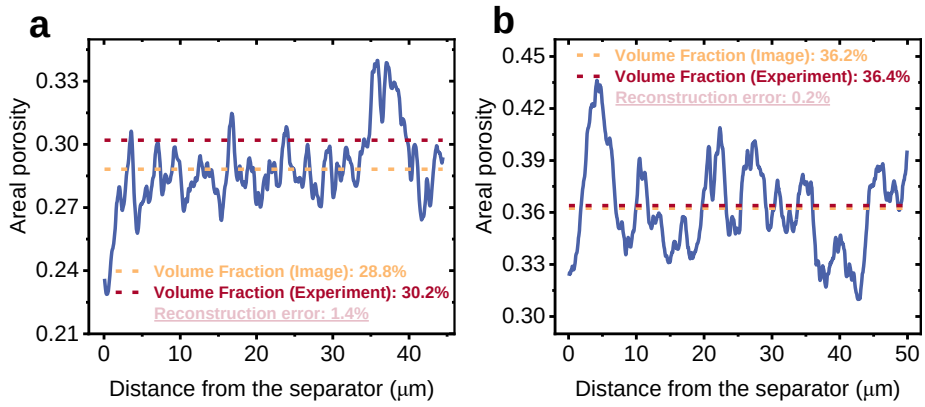

Fig. 2. Validation of reconstructed electrode microstructures based on porosity. a Cathode; b anode.

3 Calculation of electrode structure-related parameters

3.1 REVs selection

In this study, the volume sizes of cathode and anode in real world are both about 5 cm × 5cm × 60 μm. In contrast, owing to the limitations of FIB-SEM, the microstructures reconstructed in aforementioned section (40 μm × 40 μm × 40 μm) are much smaller than the actual electrodes. The analyzed microstructure size has a great effect on the calculation results of structure-related parameters. Therefore, it is necessary to select the REV which has the ability to reflect the structural characteristics of the entire electrode and reduce computational complexity to the maximum extent [19].

As depicted in Fig. 3, the ROI sizes of cathode (Fig. 3a) and anode (Fig. 3b) were gradually

increased from 100 voxels × 100 voxels × 100 voxels (3 μm × 3 μm × 3 μm) with each increment of 100 voxels (3 μm). To comprehensively represent the structural characteristics, the porosity, D50 diameter of AM, and macmullin number were selected as key indicators. Among them, the macmullin number express the limitations to charge/mass transport within electrolyte because of complex pore structure [20], which is defined as Eq. (1).

$$N_m = \frac{\sigma_l}{\sigma_{eff}} = \frac{D_l}{D_{eff}} \tag{1}$$

Where, σ_l / D_l is the conductivity/diffusion coefficient of electrolyte and σ_{eff} / D_{eff} represents the effective conductivity/diffusion coefficient of pore phase.

As basic properties of electrode microstructures, the porosity of pore phase and D50 diameter of AM phase were analyzed firstly. From the results in Fig. 3c and 3d, as the ROI sizes increase along the diagonal direction, the porosity and D50 diameter change dramatically, indicating the unconverged state. When it reaches to 900 voxels (27 μm) and 1100 voxels (33 μm) for cathode (Fig. 3c) and anode (Fig. 3d), the porosity and D50 diameter remain constant, demonstrating the converged state. Thus, the 3D microstructures with lengths of 27 μm and 33 μm were determined as the RVEs for cathode and anode, respectively. Extracting structure-related parameters based on them both reduces the computational complexity and represents the entire electrodes.

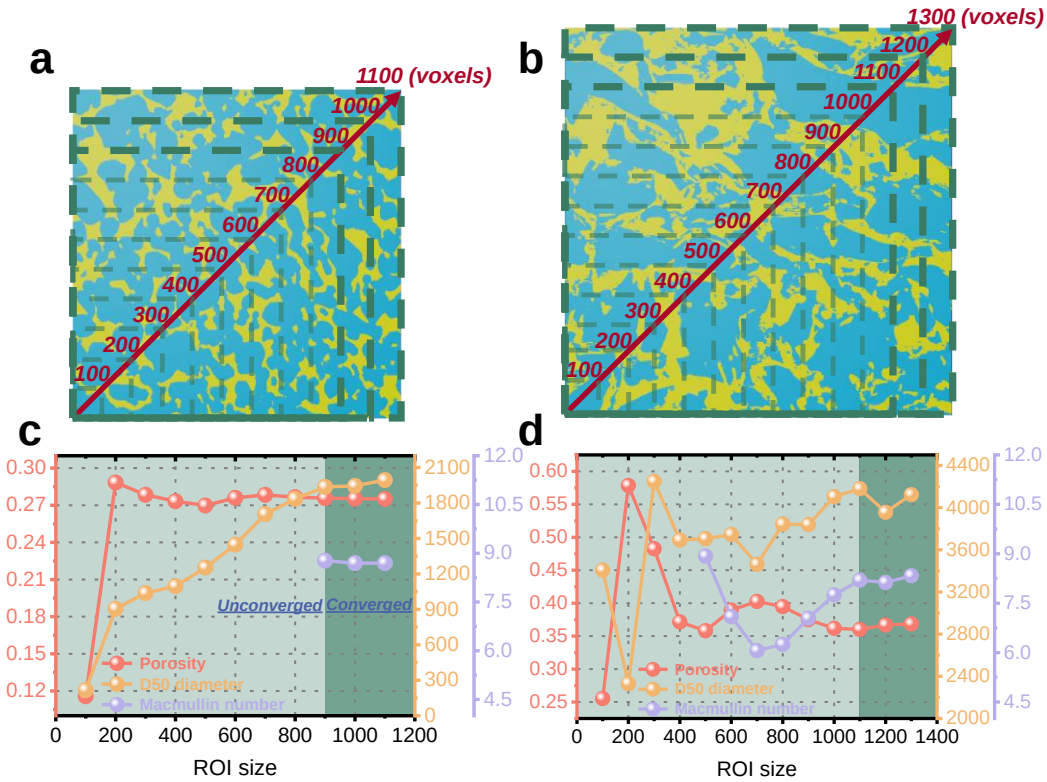

Fig. 3. REVs selection of the electrode microstructures. a, b Increased ROI size of cathode (a) and anode (b). The 2D images are shown as a schematic presentation; c, d corresponding variations of structure-related factors of cathode (c) and anode (d) with the increase of ROI size.

3.2 **Absolute permeability calculation**

Absolute permeability serves as a crucial parameter to describe the infiltration rate of electrolyte, which is only related to the pore structure morphology. To obtain it accurately, it is necessary to simulate the fluid flow behavior within pore phase at the mesoscale. Fig. 4a describes the calculation principle of absolute permeability, where the fluid is defined a low speed in the inlet boundary and the pressure is set as 0 in the outlet boundary. Besides, the remaining outer boundaries are set with symmetric properties. Considering the fact that absolute permeability is independent of the type and properties of the fluid, a simple example of water was adopted here.

In practical operation, the RVEs of cathode and anode were meshed based on detailed bitmap data. This method is particularly suitable for image-based modeling. It directly generates meshes based on individual pixels rather than combined geometric structures, which maximize the fidelity of complex porous structures. Mesh results of cathode and anode are shown in Fig. 4b and 4c, respectively, where the low skewness distribution proves the excellent mesh quality. Fig. 4d and 4e present the resulting pressure distributions of cathode and anode, respectively, and the absolute permeabilities were calculated 2.05e-15 m^2 and 3.46e-15 m^2 using Eq. (2).

$$\kappa = u_{out}\mu\frac{L}{\Delta p} \tag{2}$$

Where, u_{out} (m/s) is the flow speed in the outlet boundary, μ (Pa·s) is the dynamic viscosity of liquid, L (m) is the side length along the fluid flow direction, Δp (Pa) is the pressure difference between inlet and outlet boundaries.

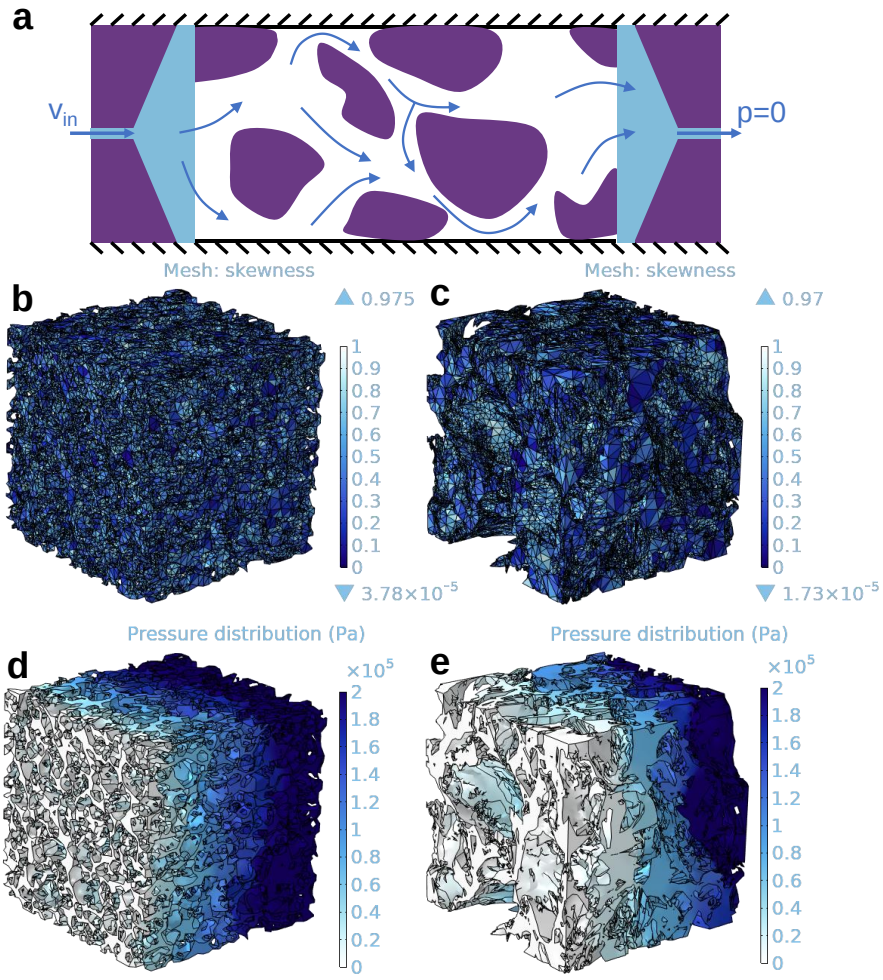

Fig. 4. Calculation principle and results of the electrode absolute permeability. a Setup of the pore-scale flow simulation; b, c mesh quality of cathode (b) and anode (c) pore structures; d, e simulation results of cathode (d) and anode (e) pore structures.

3.3 Average pore diameter acquisition

The average pore diameter is a further characterization of the pore structure based on the porosity, also playing a pivotal role in the electrolyte infiltration process. The PNM [21] is usually used to obtain the pore size distribution, in which the pores and throats are abstracted as spherical nodes and cylindrical connecting edges in the network, respectively. From Fig. 5, the PNMs of cathode RVE (Fig. 5a) and anode RVE (Fig. 5b) are shown, where the colors and diameters of the equivalent spheres are

corresponding to the pore sizes. Fig. 5c and 5d display the pore diameter distribution curves of cathode and anode, respectively, based on which the average diameters were derived 0.915 μm and 1.09 μm.

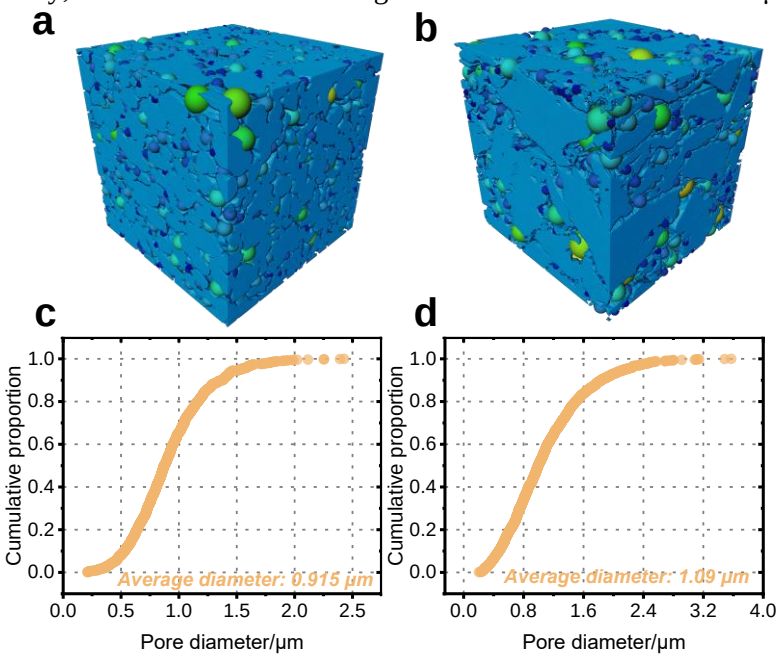

Fig. 5. Calculation principle and results of the average pore diameters. a, b PNMs of cathode (a) and anode (b). Different pores are separated and equivalent to spheres; c, d Pore size distributions and average diameters of cathode (c) and anode (d).

In summary, the structure-related parameters of cathode and anode required for electrolyte infiltration process modeling are listed in Table 1.

Table 1. Structure-related parameters of cathode and anode required in the model.

Parameter		Value
Cathode	Averaged pore radius	1.048 μm
	Porosity	27.6%
	Absolute permeability	2.05e-15 m^2
Anode	Averaged pore radius	1.27 μm
	Porosity	36%
	Absolute permeability	3.46e-15

4 Electrolyte infiltration model

4.1 Model simplification

Modeling the electrolyte infiltration process based on the whole electrode microstructures at the mesoscale is extremely difficult due to the unacceptable mesh quantity and resulting computational time. In addition, it is also challenging to obtain the entire electrode microstructures. Therefore, it is necessary to simplify the simulation task to achieve efficient application in practical engineering scenarios.

As described in Fig. 6, the y-axis and z-axis correspond to electrolyte flow direction and

electrode thickness direction, respectively. Through structure parameters extraction and transfer, this mesoscale simulation problem was simplified to modeling at macroscale, significantly reducing the computational complexity and hardware requirements. In detail, in mesoscale modeling, the pore parameters (porosity and average pore diameter) and absolute permeability were calculated based on the electrode RVEs. These parameters were then imported to the electrolyte infiltration models established at macroscale, which assumed the whole electrodes as uniformly distributed porous media.

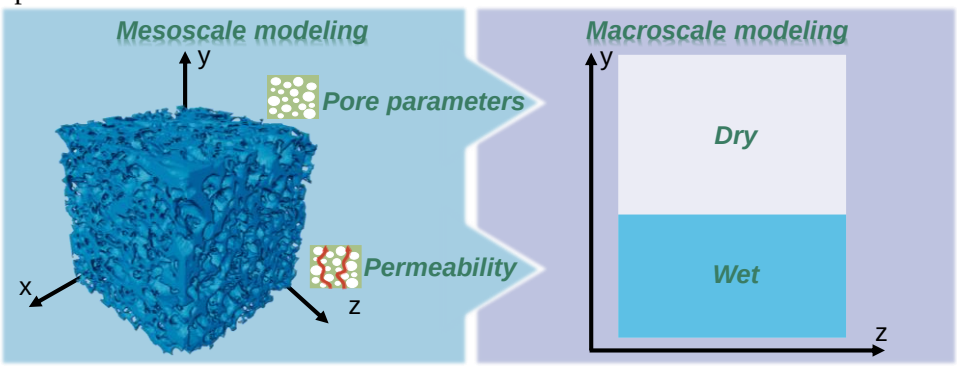

Fig. 6. Simplification of electrolyte infiltration model: from mesoscale to macroscale. Pore parameters and permeability are calculated through mesoscale modeling and imported into the macroscale model.

4.2 Fluid parameters

During the electrolyte infiltration process, the electrolyte continuously displaces the gas within pore phase. This process ought to be operated in glove-box condition which is mostly filled with nitrogen. The density and dynamic viscosity were from standard theoretical value. In contrast, as another key parameters in the model, electrolyte properties were obtained by experiments, including density, dynamic viscosity, surface tension, and contact angle. It is noteworthy that the contact angle varies for cathode and anode, requiring respective tests. Detailed results of fluid parameters are shown in Table 2. Notably, these values are all at 25°C.

Table 2. Gas and electrolyte parameters required in the model.

Fluid type	Density	Dynamic viscosity	Surface tension	Contact angle
Gas (nitrogen)	1.168 kg/m^3	1.84e-2 $mPa \cdot s$	/	/
Electrolyte	1290 kg/m^3	1.16 $mPa \cdot s$	35.945 mN/m	20° (cathode) 16.06° (anode)

4.3 Multi-physics definition

In this model, the darcy's law and multiphase transfer in porous media were considered and defined using Eq. (3-9) [22].

The volume fractions of gas and electrolyte were defined as s_1 and s_2, respectively, which follows:

$$\frac{\partial}{\partial t}(\varepsilon \rho_i s_i) + \nabla \cdot \left(-\rho_i \kappa \frac{\kappa_{ri}}{\mu_i} (\nabla p_i - \rho_i g) \right) = Q_i = 0 \tag{3}$$

$$s_1 = 1 - s_2 \tag{4}$$

Where, ε represents the porosity of pore phase, ρ_i (kg/m^3), κ (m^2), κ_{ri}, μ_i ($Pa \cdot s$), and p_i (Pa) are

fluid density, absolute permeability, relative permeability, dynamic viscosity, and fluid pressure, respectively.

According to the Brooks-Corey model, the relative permeability κ_{ri} of gas and electrolyte are:

$$\kappa_{rS_n} = \overline{s_n}^2 (1 - (1 - \overline{s_n})^{(1+2/\lambda_p)}) \tag{5}$$

$$\kappa_{rS_w} = \left(\overline{s_w}\right)^{(3+2/\lambda_p)} \tag{6}$$

Where, $\overline{s_n}$ and $\overline{s_w}$ are saturations of gas and electrolyte, respectively, and λ_p is pore size distribution index.

The capillary pressure p_c varies with the change of electrolyte saturation $\overline{s_w}$, which also follows the Brooks-Corey model as:

$$p_c = p_{ec} \frac{1}{\left(\overline{s_w}\right)^{\frac{1}{\lambda_p}}} \tag{7}$$

$$p_{ec} = \frac{2 * \gamma * \cos\theta}{R_c} \tag{8}$$

Where, p_{ec} (Pa) represents the entry capillary pressure, γ (N/m), θ, and R_c (m) are surface tension, contact angle, and average pore diameter, respectively.

The darcy's law was employed to describe the flow behavior of fluids:

$$\frac{\partial}{\partial t}(\rho\varepsilon) + \nabla \cdot \rho\left[-\frac{\kappa}{\mu}(\nabla p)\right] = 0 \tag{9}$$

4.4 Infiltration process prediction

The macroscale electrode geometries (60 mm × 55 mm × 48.5 μm for cathode and 60 mm × 55 mm × 60 μm for anode) were constructed in COMSOL software, where the aforementioned structure-related and fluid parameters, along with partial differential equations (PDEs) were coupled to establish the electrolyte infiltration model. Simulation results of cathode and anode are illustrated in Fig. 7, it is shown from Fig. 7a that the electrolyte mass infiltrated into the electrodes firstly increases and then reaches convergence over time. Two important phenomena are observed: More electrolyte is absorbed by anode compared with cathode, owing to its thicker electrode and higher porosity which result in more pore volume; The electrolyte infiltration rate within anode is faster than cathode, because of its bigger pore diameter, higher absolute permeability, and smaller contact angle that are all beneficial for electrolyte infiltration. Attached are the time-dependent variations of electrolyte saturation within the infiltration planes of cathode and anode, as shown in Fig. 7b.

It is concluded that it requires at least 3000 s (50 min) to realize the fully infiltrated state of both electrodes for this battery. It is noteworthy that the infiltration time required to reach convergence for cathode and anode is close. This is an expective phenomenon which to the maximum extent reduces the standing time and accelerates the manufacturing efficiency in practical scenarios.

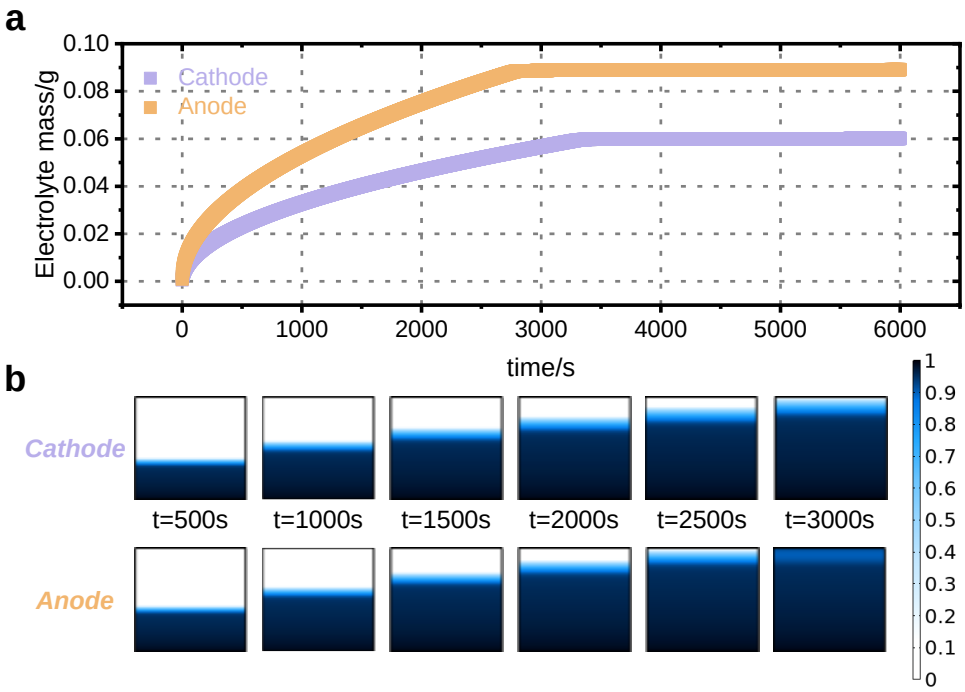

Fig. 7. Simulated electrolyte infiltration processes within cathode and anode. a Mass curves of the electrolyte infiltrated into the electrodes; b time-dependent diagrams of electrolyte saturation on the infiltration plane.

5 Conclusions

In this study, we carried out cross-scale analysis from mesoscale to macroscale, to establish an electrolyte infiltration model that coupled microstructure characteristics into the simplified uniformly distributed model. Assisted by FIB-SEM, the 3D microstructures of cathode and anode were reconstructed and validated accurate based on porosity. Through selecting key structural parameter indicators, the RVEs of both electrodes were determined. Based on which, we acquired the absolute permeability and average pore diameter using FEM and PNM. These structure-related parameters (porosity, permeability, and average pore diameter) and experimental tested electrolyte parameters were imported to the macroscale electrolyte infiltration model, which was described by multiphase transfer in porous media and darcy's law. Results showed that it required at least 50 min to get the entire electrodes infiltrated. Besides, because the anode microstructure with bigger pore diameter was more beneficial for electrolyte flow, it reached the convergence state earlier than cathode, despite a larger pore volume. The proposed model provides valuable insights into the understanding and optimization of electrolyte infiltration process for batteries to enhance the manufacturing efficiency.

Acknowledgments

This work is financially supported by the Fundamental Research Funds for the Central Universities and the Major State Basic Research Development Program of China (973 Program, Grant No. 2022YFB2502302, Grant No. 2022YFB2502304).

References

[1] LIU C,LOMBARDO T,XU J, et al.An experimentally-validated 3D electrochemical model revealing electrode manufacturing parameters' effects on battery performance[J].Energy Storage Mater,2023,54:156-63.
[2] CUI H,SONG Y,REN D, et al.Electrocapillary boosting electrode wetting for high-energy lithium-ion batteries[J].Joule,2024,8:29-44.
[3] FANG R,DONG P,GE H, et al.Capacity plunge of lithium-ion batteries induced by electrolyte drying-out: Experimental and Modeling Study[J].J Energy Storage,2021,42:
[4] GüNTER F J,RöSSLER S,SCHULZ M, et al.Influence of the Cell Format on the Electrolyte Filling Process of Lithium-Ion Cells[J].Energy Technology,2019,8:

[5] WEYDANZ W J,REISENWEBER H,GOTTSCHALK A, et al.Visualization of electrolyte filling process and influence of vacuum during filling for hard case prismatic lithium ion cells by neutron imaging to optimize the production process[J].J Power Sources,2018,380:126-34.
[6] SCHILLING A,GüMBEL P,MöLLER M, et al.X-ray Based Visualization of the Electrolyte Filling Process of Lithium Ion Batteries[J].J Electrochem Soc,2018,166:A5163-A7.
[7] DENG Z,HUANG Z,SHEN Y, et al.Ultrasonic Scanning to Observe Wetting and “Unwetting” in Li-Ion Pouch Cells[J].Joule,2020,4:2017-29.
[8] CAI J,WEI X,WANG X, et al.Revealing effects of pouch Li-ion battery structure on fast charging ability through numerical simulation[J].Applied Energy,2025,377:
[9] CHEN F,LU K,CHEN T, et al.Multiscale simulation and AI techniques for optimizing electrolyte injection processes[J].Cell Reports Physical Science,2025,6:
[10] CHEN F,CHEN T,WU Z, et al.Unraveling Mechanisms of Electrolyte Wetting Process in Three-Dimensional Electrode Structures: Insights from Realistic Architectures[J].Green Energy and Intelligent Transportation,2025,
[11] LAUTENSCHLAEGER M P,PRIFLING B,KELLERS B, et al.Understanding Electrolyte Filling of Lithium-Ion Battery Electrodes on the Pore Scale Using the Lattice Boltzmann Method[J].Batteries & Supercaps,2022,5:
[12] LEE S G,JEON D H,KIM B M, et al.Lattice Boltzmann Simulation for Electrolyte Transport in Porous Electrode of Lithium Ion Batteries[J].J Electrochem Soc,2013,160:H258-H65.
[13] SHODIEV A,PRIMO E,ARCELUS O, et al.Insight on electrolyte infiltration of lithium ion battery electrodes by means of a new three-dimensional-resolved lattice Boltzmann model[J].Energy Storage Mater,2021,38:80-92.
[14] GüNTER F J,KEILHOFER J,RAUCH C, et al.Influence of pressure and temperature on the electrolyte filling of lithium-ion cells: Experiment, model and method[J].J Power Sources,2022,517:
[15] CHEN H-S,YANG S,SONG W-L, et al.Quantificational 4D visualization and mechanism analysis of inhomogeneous electrolyte wetting[J].Etransportation,2023,16:
[16] WU Z,CHEN F,ZHOU Z, et al.Data-driven macro-scale simulation for rapid electrolyte wetting in lithium-ion batteries[J].J Energy Storage,2025,106:
[17] GHADBAN M,SABHARWAL M,REA C, et al.3D microscale modeling of NMC cathodes using multi-resolution FIB-SEM tomography[J].J Power Sources,2023,562:
[18] LU X,BERTEI A,FINEGAN D P, et al.3D microstructure design of lithium-ion battery electrodes assisted by X-ray nano-computed tomography and modelling[J].Nat Commun,2020,11:2079.
[19] XU H,ZHU J,FINEGAN D P, et al.Guiding the Design of Heterogeneous Electrode Microstructures for Li-Ion Batteries: Microscopic Imaging, Predictive Modeling, and Machine Learning[J].Adv Energy Mater,2021,11:
[20] YAN Z,WANG L,ZHANG H, et al.Determination and Engineering of Li-Ion Tortuosity in Electrode Toward High Performance of Li-Ion Batteries[J].Adv Energy Mater,2024,14:
[21] KHAN Z A,AGNAOU M,SADEGHI M A, et al.Pore Network Modelling of Galvanostatic Discharge Behaviour of Lithium-Ion Battery Cathodes[J].J Electrochem Soc,2021,168:
[22] MASOODI R,PILLAI K M.Darcy's law-based model for wicking in paper-like swelling porous media[J].AIChE Journal,2010,56:2257-67.

Presenter Biography

Jixiang Cai received the B.S. degree in School of Mechanical and Automotive Engineering at South China University of Technology, China, in 2021. Currently, he is studying for the Ph. D. degree in the School of Automotive Studies, Tongji University, China. His research interests include multiscale and multiphysics lithium-ion battery modeling, relationship between electrode microstructure and performance, AI for batteries.